nature ecology & evolution

ARTICLES

https://doi.org/10.1038/s41559-020-01319-6

Drimolen cranium DNH 155 documents microevolution in an early hominin species

Jesse M. Martin[1,11], A. B. Leece[1,11], Simon Neubauer[2], Stephanie E. Baker[3], Carrie S. Mongle[4,5], Giovanni Boschian[3,6], Gary T. Schwartz[7], Amanda L. Smith[8], Justin A. Ledogar[9], David S. Strait[3,10] ✉ and Andy I. R. Herries[1,3]

Paranthropus robustus **is a small-brained extinct hominin from South Africa characterized by derived, robust craniodental morphology. The most complete known skull of this species is DNH 7 from Drimolen Main Quarry, which differs from *P. robustus* specimens recovered elsewhere in ways attributed to sexual dimorphism. Here, we describe a new fossil specimen from Drimolen Main Quarry, dated from approximately 2.04–1.95 million years ago, that challenges this view. DNH 155 is a well-preserved adult male cranium that shares with DNH 7 a suite of primitive and derived features unlike those seen in adult *P. robustus* specimens from other chronologically younger deposits. This refutes existing hypotheses linking sexual dimorphism, ontogeny and social behaviour within this taxon, and clarifies hypotheses concerning hominin phylogeny. We document small-scale morphological changes in *P. robustus* associated with ecological change within a short time frame and restricted geography. This represents the most highly resolved evidence yet of microevolutionary change within an early hominin species.**

Drimolen Main Quarry (DMQ) is a palaeocave in the Gauteng Province exposures of the Malmani Dolomite, approximately 40 km north-west of Johannesburg in South Africa[1–3] (Fig. 1). DNH 155 was recovered from in situ partially decalcified, clast-supported breccia derived from 3.24 to 3.56 m below, 198.360 south, and 214.117 west of the site datum in the basal part of the central talus cone of DMQ dating to between approximately 2.04 and 1.95 million years ago[3] (Ma; Fig. 1). The specimen was found approximately 2.4–2.8 m below a thin speleothem (Walls of Jericho flowstone) that has been dated by uranium–lead to approximately 1.96 ± 11 Ma[3,4] and formed within a magnetic reversal at the base of the Olduvai Subchron at approximately 1.95 Ma[3] (Fig. 1d). DNH 155 was found 1.6–2.0 m below the base of this reversal and 1.6–2.0 m above a uranium series electron spin resonance date of 2.04 ± 0.24 Ma[3], indicating an age of approximately 2 Ma (Fig. 1d). A recently described[3] less complete male cranium, DNH 152, was recovered in situ from a lateral stratigraphic equivalent of the same talus cone at −3.15 m and is thus of a comparable age[3]. DNH 7 was recovered in 1994[1] from a large decalcifying breccia block that also probably derives from the same part of the talus cone but has collapsed and so is no longer in situ[3]. DNH 155 (Fig. 2 and Extended Data Fig. 1) and DNH 7 preserve a suite of primitive and derived traits collectively compatible with an allocation to *Paranthropus robustus*. (We note that Y. Rak and W. Kimbel are independently describing and reconstructing DNH 7.) These include: large postcanine teeth; small incisors and canines; an anteriorly shallow palate; a maxillary trigon; a maxillary fossula; a zygomaticomaxillary fossa; infraorbital foramina positioned low on the face; broad and somewhat flattened anterior pillars that are solid internally; a deep temporomandibular joint; a small postglenoid process fused to a vertical tympanic plate; a large circular external auditory meatus; and pneumatized temporal squamae. DNH 155 further resembles *P. robustus* in traits not preserved in DNH 7, including a thick palate that overlaps the clivus and a smooth nasal cavity entrance. DNH 152 preserves much less morphology but resembles either or both specimens with respect to the traits that can be observed. DNH 7 has previously been allocated to *P. robustus*[1] and that assignment has never been questioned.

Results

Despite their similarities, DNH 155, DNH 7 and (when the relevant morphology is preserved) DNH 152 differ in substantial ways from *P. robustus* specimens from the Swartkrans Member 1 Hanging Remnant and Kromdraai B (the species is also found at Cooper's D, Sterkfontein Member 5B, Gondolin and other units at Swartkrans but most fossils from these deposits are fragmentary) (Supplementary Table 1 and Supplementary Fig. 1). Robust australopiths from the Swartkrans Member 1 Hanging Remnant have at times been referred to *Paranthropus crassidens*[5–7] but this taxonomy is not conventional and the Swartkrans Member 1 Hanging Remnant and Kromdraai B samples have generally been considered conspecific after exhaustive analysis of their dentitions[8,9]. Some of the differences between the DMQ robust australopiths and those from other sites pertain to feeding biomechanics (Supplementary Information); insofar as mechanical performance may be the target of selection (see, for example, ref. [10]), they may reflect subtle differences in feeding adaptations. Adult male *P. robustus* from Swartkrans Member 1 Hanging Remnant have an anteriorly positioned sagittal crest arising on

[1]Palaeoscience, Department of Archaeology and History, La Trobe University, Bundoora, Victoria, Australia. [2]Max Planck Institute for Evolutionary Anthropology, Department of Human Evolution, Leipzig, Germany. [3]Palaeo-Research Institute, University of Johannesburg, Auckland Park, Johannesburg, South Africa. [4]Division of Anthropology, American Museum of Natural History, New York, NY, USA. [5]Turkana Basin Institute, Stony Brook University, Stony Brook, NY, USA. [6]Department of Biology, University of Pisa, Pisa, Italy. [7]Institute of Human Origins, School of Human Evolution and Social Change, Arizona State University, Tempe, AZ, USA. [8]Department of Organismal Biology & Anatomy, The University of Chicago, Chicago, IL, USA. [9]Department of Evolutionary Anthropology, Duke University, Durham, NC, USA. [10]Department of Anthropology, Washington University in St. Louis, St. Louis, MO, USA. [11]These authors contributed equally: Jesse M. Martin, A. B. Leece. ✉e-mail: dstrait@wustl.edu

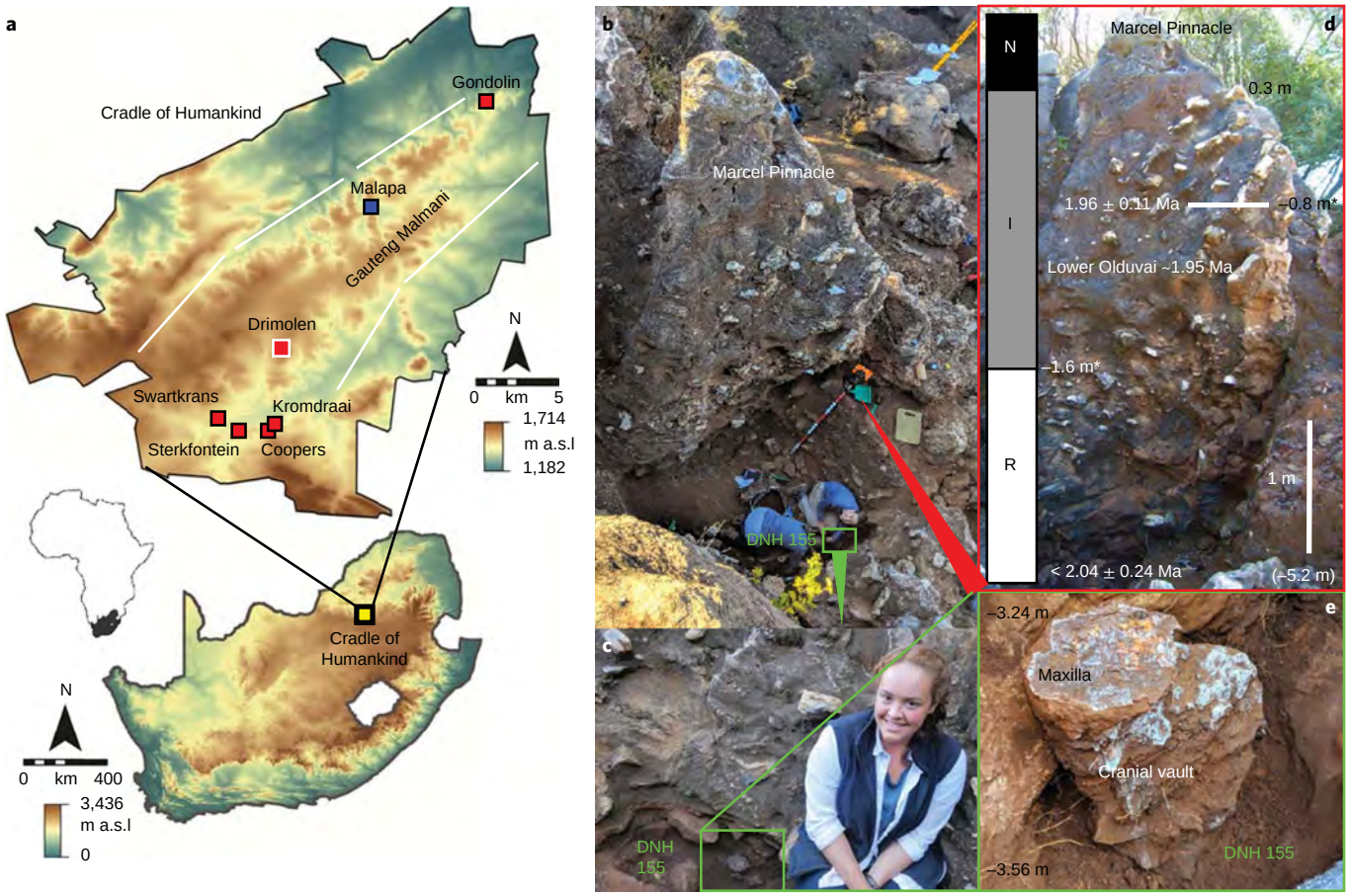

Fig. 1 | Geographical and stratigraphic context of DNH 155. a, Location of Drimolen within the Gauteng Province exposure of the Malmani Dolomite (designated in this figure as the Gauteng Malmani and outlined in white) near Johannesburg, South Africa. *Paranthropus*-bearing sites are highlighted in red and the contemporary *Australopithecus*-bearing site of Malapa in blue. a.s.l, above sea level. **b**, Vertical view of the location of DNH 155 during excavation (S.B. and A.L. excavating) in breccia south of and below the base of the Marcel Pinnacle on the western side of DMQ. **c**, Location of the DNH 155 cranium within a pocket of decalcified sediments within an in situ remnant of the central talus cone breccia (fossil discoverer S. Good pictured) that connects between the western dolomite wall of the cave, the Marcel Pinnacle and the top of the Jangi Buttress. The green arrow in **b** indicates the angle from which the photo was taken. **d**, Longitudinal (east–west) profile of the Marcel Pinnacle southern face, showing the internal structure of the talus cone and projected (indicated by the single asterisk) locations (depth from datum in metres) of palaeomagnetic data and radiometric dates from the Walls of Jericho Pinnacle on the northern side of the Marcel Pinnacle. The red arrow in **b** indicates the angle from which the photo was taken. **e**, The DNH 155 cranium during excavation and just before removal of its attachment to the breccia is shown, with the depth below the datum in metres.

the frontal bone[11], presumably reflecting extreme hypertrophication of the anterior fibres of the temporalis. In contrast, DNH 155 and DNH 152 exhibit crests that arise somewhat more posteriorly. DNH 7 and DNH 155 also exhibit more posteriorly positioned zygomatic roots relative to the tooth row than robust australopiths from the Swartkrans Member 1 Hanging Remnant and Kromdraai B (Extended Data Fig. 2). Root position coarsely approximates masseter muscle leverage[12–14], so evidence from the sagittal crest and zygomatic root suggests that *P. robustus* from DMQ was less efficient at producing bite force than *P. robustus* from other sites. Moreover, the palate of DNH 155 protrudes anterior to sellion to a greater degree than in any other *P. robustus* specimen[12,15] (Supplementary Table 2), positioning the teeth farther away from the articular eminence and further decreasing bite force efficiency. Indeed, the leverage of the masseter muscle is quantitatively less in DNH 155 during bites on the M^3 than in any measured *P. robustus* or *Paranthropus boisei* specimen (Supplementary Information and Supplementary Table 2); the masseter of *P. robustus* specimen SK 48 would have been nearly 50% more efficient at creating bite force at the M^3 than that of DNH 155. Finally, the zygomatic root is antero-posteriorly thin in DNH 7 and DNH 155. In contrast, the root expands posteriorly to encompass most of the maxilla in other adult *P. robustus* (Extended Data Fig. 3) and may be more efficient at dissipating shear stresses as the maxilla experiences a superiorly directed bite force just medial to an inferiorly directed masseter force, particularly when the zygomatic root is positioned especially far anteriorly (Supplementary Information and Supplementary Figs. 2 and 3).

Further differences between the DMQ robust australopiths and *P. robustus* from other sites lack obvious functional roles and may represent selectively neutral distinctions between populations. DNH 7 and DNH 155 have more sagittally oriented petrous bones than any other *Paranthropus* specimens (Supplementary Table 3). They also lack a zygomaticomaxillary step (Extended Data Fig. 4) and differ from all other adult *P. robustus* in having rounded rather than squared supraorbital corners with sloping rather than horizontal superior orbital margins, a trait also seen in DNH 152 (Extended Data Fig. 5). Although the configuration of the orbital margin has been claimed to have biomechanical significance in relation to feeding[12], modelling experiments do not support that view (Supplementary Information and Supplementary Fig. 4).

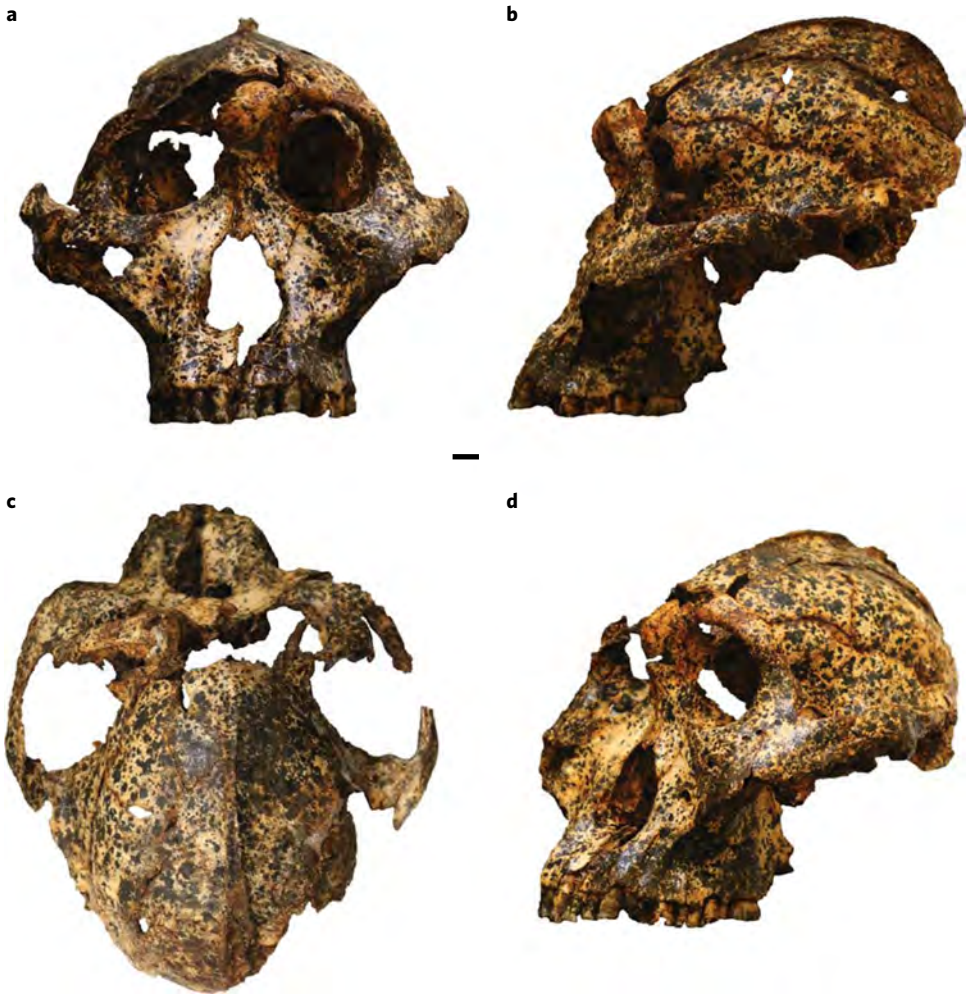

Fig. 2 | Specimen DNH 155. a–d, Specimen photographed in frontal (**a**), left lateral (**b**), superior (**c**) and oblique (**d**) views. Scale bar, 10 mm. The specimen is so fragile that it is difficult to position precisely in standard views. Accordingly, additional views in the form of surface scans are presented in Extended Data Fig. 1.

Cluster analysis of factor scores derived from a principal component analysis (PCA) based on 19 size-adjusted linear dimensions confirm that DNH 7 and DNH 155 are metrically similar to each other and distinct within a *Paranthropus* cluster (Extended Data Fig. 6). Note that the cluster analysis explains 100% of the variance in the measurements and thus outweighs patterning from any one or pair of principal components.

Endocranial volume in DNH 155 can be estimated with a high degree of confidence (Supplementary Fig. 5) using geometric morphometric methods[16–18]. Multiple estimates yielded endocranial volumes centred around 450 ml with narrow confidence limits. DNH 155 is thus at the lower end of variation in *P. robustus*, which ranges conservatively from 465 to 530 ml (ref. [19]). Preserved portions of the endocranial cavities of DNH 7 and DNH 152 appear to be qualitatively similar in size to that of DNH 155.

DNH 155 differs from DNH 7 in ways probably representing sexual dimorphism and is interpreted to be male. In addition to being absolutely larger in size, it exhibits strong anteromedial incursion of the superior temporal lines, a sagittal crest and a zygomatic that protrudes anterior to the nasal cavity margin (Extended Data Fig. 7).

As described above, robust australopiths from DMQ preserve a suite of primitive and derived character states unlike those seen in other robust taxa. When the DMQ robust australopith sample is treated as an independent taxon in both Bayesian and maximum parsimony phylogenetic analyses (Fig. 3a, Supplementary Fig. 6 and Supplementary Information), it is positioned as the basal member of the *Paranthropus* clade. Notably, *Paranthropus aethiopicus* is positioned as the sister taxon of *P. boisei*, implying the existence of an eastern African robust clade. The position of the DMQ taxon is counterintuitive insofar as this sample post-dates *P. aethiopicus* by hundreds of thousands of years. To evaluate the effect of chronology on the phylogenetic relationships among robust australopiths, a tip-dated Bayesian analysis was performed on the *Paranthropus* clade. By incorporating stratigraphic information directly into our estimation of evolutionary relationships among the robust australopiths, we recover a moderately supported tree that suggests distinctly divergent eastern and southern African robust clades (Fig. 3b). A common finding of all analyses is that the last common ancestor of *Paranthropus* probably predates *P. aethiopicus* and that the known eastern and southern African robust australopiths may have diverged early in the history of the robust clade. There is no compelling evidence from these results suggesting that *Australopithecus africanus* is the direct ancestor of *P. robustus*[20–24].

The traits distinguishing robust australopiths at DMQ from those at other sites are drawn from several distinct functional and developmental modules of the cranium and vary independently in robust australopiths (Supplementary Table 1), so the differences cannot be dismissed as a correlated change in a single character complex. Rather, they appear to represent some level of meaningful differentiation among palaeopopulations. Critically, it

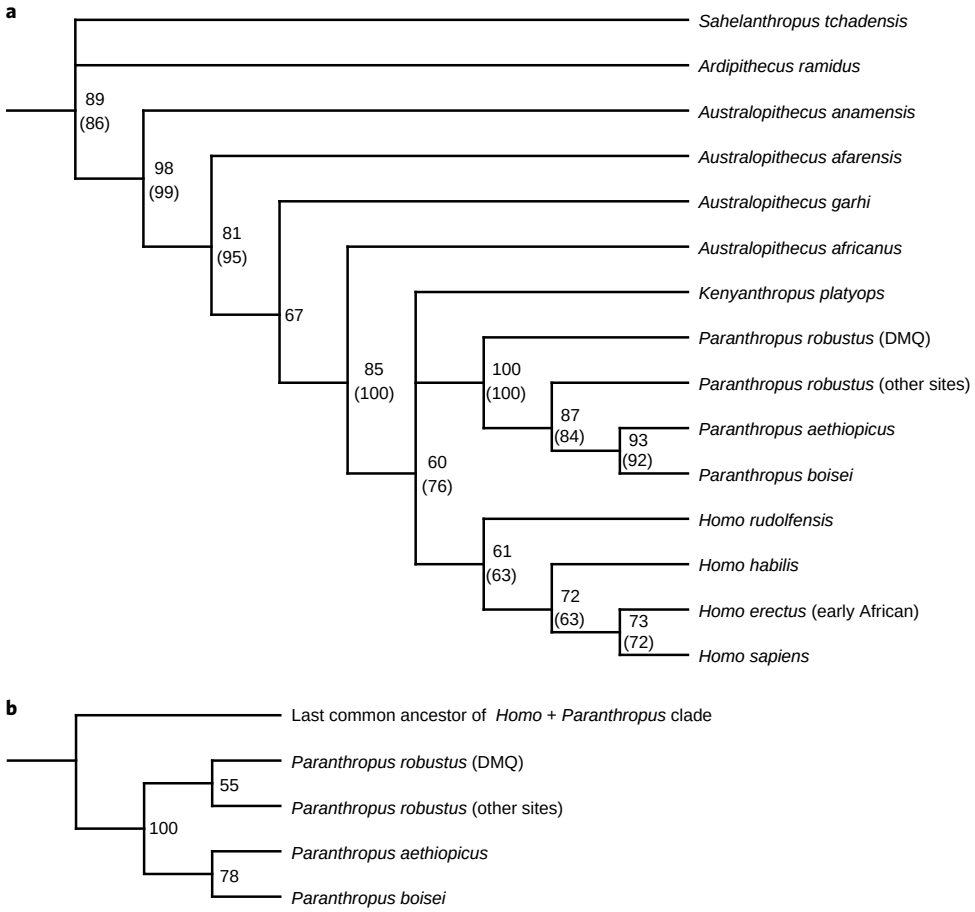

Fig. 3 | Phylogenetic relationships of early hominins while treating the DMQ robust australopiths as a distinct taxon. a, Maximum-credibility majority-rule ('halfcompat') tree from Bayesian inference analysis of a character matrix modified from a previous study[70]. Values at the nodes represent posterior probabilities (%); values in parentheses represent posterior probabilities when *Kenyanthropus platyops* and *Australopithecus garhi* (both of which are missing data with respect to many characters) are excluded from the analysis. Maximum parsimony analysis recovered a single, nearly identical, most parsimonious tree (Supplementary Information). **b**, Maximum-credibility majority-rule ('halfcompat') tree from tip-dated Bayesian inference analysis. The character states of the outgroup taxon, representing the last common ancestor of the *Homo* + *Paranthropus* clade, were reconstructed using maximum parsimony.

is unlikely that these samples could have been drawn from populations sharing common statistical parameters (Supplementary Information). Moreover, geography cannot explain the differences among South African robust australopiths since DMQ is separated from Swartkrans Member 1 Hanging Remnant and Kromdraai B by less than 6.3 km (Fig. 1), a distance comparable to the home range of a single chimpanzee community consisting of only a few dozen individuals[25]. Remaining plausible explanations include temporally patterned variation within a single species or variation between two species. Temporally patterned variation is plausible because DMQ broadly predates Swartkrans Member 1 Hanging Remnant, which is probably close in age to a 1.8-Ma capping speleothem[26,27]. Kromdraai B has not been subject to radiometric dating so its age is less certain. A preliminary assessment suggested an age of approximately 1.78 Ma for Member 2 and less than 1.78 Ma for the Member 3 hominin-bearing deposits[27]. Subsequent work has called into question the relationships of palaeomagnetic samples to particular Members[28], the sequencing of which has recently been revised[29]. Although we cannot at present rule out the possibility that there was some brief overlap in time during which sediments were accumulating in all of the caves, it is nonetheless reasonable to consider the DMQ fossil sample to broadly predate those of Swartkrans Member 1 Hanging Remnant and Kromdraai B. Note that temporally patterned variation is not necessarily the same phenomenon as a trend; the mean value of a species might oscillate over time without producing a trend, yet the differences between populations at any two given times would nonetheless be real. Thus, we are not suggesting that the differences between the DMQ and Swartkrans Member 1 Hanging Remnant assemblages are necessarily part of a long-term trend that predates and/or postdates these deposits. Rather, we simply note that the two samples are morphologically distinct and are not contemporaneous on the landscape.

Regardless of the relative ages of the caves, current taxonomic practice in palaeoanthropology would justify the recognition of the DMQ robust australopiths as a distinct species. As a matter of practice, most new hominin species are defined almost exclusively by morphological diagnosability (see, for example, refs. [30–36]) and the DMQ sample is diagnosably distinct from the Swartkrans Member 1 Hanging Remnant and Kromdraai B samples (and all other hominin taxa). Yet, it has long been understood that species are parts of lineages[37–39], which are sequences of metapopulations linked by ancestry and descent. However, a species is not simply a lineage because a lineage transcends species boundaries. For example, the human lineage includes *Homo erectus* and, probably, *Australopithecus afarensis*. Thus, a species is a portion of a lineage, namely, a metapopulation lineage segment extending from initial divergence to eventual extinction, whose evolutionary history is independent of other such lineage segments[38,39]. This

definition suggests that multiple species should be delimited only when the null hypothesis of a single lineage segment can be falsified. Morphological diagnosability alone is insufficient to falsify this null hypothesis when fossil assemblages have non-overlapping temporal ranges because it is expected that morphological change may occur within a single lineage segment (Supplementary Information and Supplementary Fig. 7). Given the non-overlapping temporal ranges of the DMQ and the other robust australopith sites, we cannot falsify the hypothesis that the DMQ robust sample represents an early part of the *P. robustus* lineage segment and we adopt this as a conservative interpretation of the evidence (Supplementary Information). We suggest that palaeoanthropology has become uncritically reliant on diagnosability when delimiting species and that as a result hominin taxonomy is in danger of becoming typological. Indeed, the influence of diagnosability on palaeoanthropological thinking is so strong that even when plausible evidence is presented of evolutionary change within a single putative lineage segment (see, for example, refs. [40,41]), it remains conventional (although not universal) to attribute the early and late assemblages of fossils to different species (for example, *Australopithecus anamensis* and *Au. afarensis*; *P. aethiopicus* and *P. boisei*).

Discussion

Given the likelihood that DNH 155 is a male, one can test a hypothesis (Supplementary Information) regarding sexual dimorphism, ontogeny and social organization in *P. robustus*[11,42]. That hypothesis was based on the premise that the small size of DNH 7 could be used as a guide to help discriminate males from females at Swartkrans Member 1 Hanging Remnant and Kromdraai B. It was determined[11] that 14 of 17 fossils preserving maxillofacial morphology at Swartkrans Member 1 Hanging Remnant were males, a finding that was deemed unlikely to have occurred from random sampling. Among those males, the largest individuals (based on a metrical index of facial dimensions) were also judged to be ontogenetically the oldest based on the degree of tooth wear. These findings led to the hypothesis that *P. robustus* exhibited bimaturism where males exhibited prolonged periods of growth producing extreme levels of sexual dimorphism, presumably as an adaptation to a social organization (for example, single-male multi-female groups) where there was high male–male competition[11]. Such an organization and associated social structures (for example, dominance hierarchy, differences in male and female dispersal patterns) would have led to high predation rates in smaller non-dominant males, hence the higher representation of males in carnivore-accumulated fossil assemblages[11] of which Swartkrans Member 1 Hanging Remnant was inferred to have been[43]. It has further been proposed that dental size differences between the DMQ and Swartkrans Member 1 Hanging Remnant samples are consistent with this hypothesis insofar as the dental dimensions of most teeth are significantly larger in the latter than in the former[42], potentially corroborating the differential representation of males and females at the two sites.

The above hypothesis is not supported by the discovery of DNH 155. The facial index previously used to sort *P. robustus* maxillae into size categories[11] shows that DNH 155 is smaller than all measured presumed males from Swartkrans Member 1 Hanging Remnant (see Methods). Yet, molar wear in DNH 155 is as great or greater than that of any relevant Swartkrans Member 1 Hanging Remnant specimen per the criteria outlined in Lockwood et al.[11]. Thus, bimaturism cannot explain the relatively small size of DNH 155, thereby implying that facial size is systematically larger in the Swartkrans Member 1 Hanging Remnant population. Moreover, dental dimensions of the maxillary teeth of DNH 155 fall within or near the range of other robust australopith teeth from DMQ[42] (Extended Data Fig. 8) and corroborate the distinctively small size of the DMQ sample, irrespective of sex. As a result, a comparison of DNH 7 and DNH 155 is more likely to provide a meaningful assessment of palaeopopulation-level sexual dimorphism than a comparison between DNH 7 and any Swartkrans Member 1 Hanging Remnant male. A palaeopopulation distinction between the DMQ and Swartkrans Member 1 Hanging Remnant samples is further strengthened by the presence of morphological differences not obviously related to dimorphism (Supplementary Table 1). Consequently, sex assignments at Swartkrans Member 1 Hanging Remnant based on an assessment of female size calibrated using DNH 7 should be reconsidered, particularly regarding specimens of intermediate size that had previously been considered male[11]. Rather, it seems probable that at least some of these specimens represent females of that population, as originally proposed[6]. Uncertainty regarding the sex of these specimens weakens the posited association in males between size and age (as inferred by tooth wear) and arguably removes the basis for inferring bimaturism in this species. Dimorphism is undoubtedly present in robust australopiths from both DMQ and Swartkrans Member 1 Hanging Remnant, but perhaps not to such a degree as previously surmised[11]. Thus, the presence of a small, ontogenetically old male at the DMQ removes the need to construct complicated nested hypotheses positing bimaturism and taphonomic bias related to social behaviour to explain differences between the DMQ and Swartkrans Member 1 Hanging Remnant samples. A simpler explanation is that there has been a phyletic increase in facial and postcanine size within *P. robustus*, assuming that the DMQ and Swartkrans Member 1 Hanging Remnant assemblages are representative samples of the species.

It has long been understood that a transition took place in southern African fauna (including hominins) between the time periods represented by Sterkfontein Member 4 (2.61–2.07 Ma[44]) and Swartkrans Member 1 Hanging Remnant, and that this change occurred as the environment shifted from being more mesic to more xeric[45]. Recent advances in chronology[3,4] place DMQ squarely in the middle of this transitional period and provide further evidence for the potential role of climate change and/or instability in driving hominin evolution. Regional records indicate a significant climatic shift occurring around 2.2 Ma[46]. Local environmental records indicate a shift to drier conditions after 2.6 Ma but with more rapidly fluctuating wetter and drier episodes between approximately 2.2 Ma and approximately 2.0 Ma[4,47]. Trace element analysis indicates that *Au. africanus* from Sterkfontein Member 4 was under dietary stress that may be related to such ecological instability[48]. DMQ sediments[3] immediately follow Sterkfontein Member 4 at the start of another dry period[4] and preserve the first and last appearance dates of several extinct mammals[3] as well as the first appearance dates of *P. robustus* and *H. erectus*. Contemporaneous sediments at Malapa[49] preserve the only occurrence of *Australopithecus sediba* and the last appearance date of *Australopithecus*. Finally, Swartkrans Member 1 Hanging Remnant occurs perhaps 100–200 ka later[26] and lacks some fauna that went extinct in the intervening time[3]. Thus, *P. robustus* at DMQ appears at the onset of a comparatively dry period that extends into Swartkrans Member 1 Hanging Remnant within a context of broader faunal turnover after landscape-scale ecological instability. These ecological conditions provide the background for morphological change in the *P. robustus* lineage segment. Those changes are modest in scale but occur over a short time span. While genetic drift cannot be ruled out as a contributory causal agent, we hypothesize that at least those morphological changes that are functionally related to the performance of the feeding apparatus (Supplementary Information) are dietary adaptations. Specifically, we infer (but cannot prove) that they resulted from ecologically driven directional or, perhaps, variability[50] selection favouring increased efficiency at producing and withstanding higher bite forces. This probably expanded the *P. robustus* dietary niche to include more foods that are mechanically challenging to process, allowing increased ecological generalization[51–53]. In principle, such a selection hypothesis could be tested using quantitative genetics (see, for example, ref. [54]), although

this approach is complicated by an inability to directly measure the variance/covariance structure of extinct hominin populations. The discovery of fossil assemblages intermediate in age between DMQ and Swartkrans Member 1 Hanging Remnant would also allow a test of this selection hypothesis by documenting the correlation (or lack thereof) of very-small-scale morphological and environmental changes. Importantly, however, not all of the differences between the DMQ and Swartkrans Member 1 Hanging Remnant robust australopiths can definitively be explained by selection because traits lacking obvious performance benefits may be selectively neutral (or, in any case, the selective benefits of those traits are unknown). Other evolutionary processes, including genetic drift, may be responsible for those differences. Finally, fossil evidence suggests that some of the morphological differences between the DMQ and Swartkrans Member 1 Hanging Remnant *P. robustus* samples may have occurred through heterochrony; there is one subadult cranium from the Swartkrans Member 1 Hanging Remnant (specimen SK 52) that preserves facial morphology differing from that of Swartkrans Member 1 Hanging Remnant adults but resembling DMQ adults in certain traits (Supplementary Information and Supplementary Fig. 8). This suggests that modifications in the timing and/or rate of growth may have produced a peramorphic adult morphology in post-DMQ *P. robustus* populations and that these changes manifest themselves late in ontogeny between second molar emergence and adulthood. Peramorphosis could also explain the differences in facial size between the DMQ and later robust australopiths. More fossil evidence is needed to test this hypothesis.

Microevolution refers, in its broadest sense, to change within species (see, for example, ref. [55]). Tight chronological and geographical control combined with an enhanced understanding of palaeoenvironments and faunal communities provide us with an unparalleled window into the microevolutionary history of *P. robustus*. Although we cannot claim to see changes in allele frequencies over time, and although putative anagenetic change has been demonstrated in other early hominin lineages[40,41,56], the record of no other early hominin species preserves evidence on such a fine scale of microevolutionary change in morphology between phyletically linked palaeopopulations.

Methods

Estimation of endocranial volume (ECV). Based on surface scans of the original fossil acquired through the use of an Artec Space Spider scanner, we extracted the preserved endocranial surface of DNH 155 and generated a partial virtual endocast by smoothly filling in missing regions. We used a symmetric template of an endocranial landmark configur tion[57,58] (935 landmarks and sliding semi-landmarks; Supplementary Fig. 5) and defi ed which landmarks and sliding semi-landmarks were preserved and which were missing. Semi-landmarks were slid to the symmetric template configur tion to gain point-to-point correspondence between individuals using the bending energy of the thin-plate spline algorithm as a minimization criterion. Endocranial landmarks and semi-landmarks were also captured for an extant reference sample including 52 chimpanzees, 56 gorillas and 43 orangutans.

On the basis of the extant reference sample, a multiple linear regression model[17] was established to estimate ECV from the endocranial form of the preserved regions of DNH 155 as captured from the landmarks. The ECV of DNH 155 was predicted to be 451 ml with a single prediction interval from 425 to 475 ml. Additionally, the missing portions of DNH 155's endocranial surface were reconstructed based on thin-plate spline warping of the extant reference sample and the reconstruction ECVs were measured. The average or most common value and the range of estimates based on different reference individuals can be interpreted as the most probable value and estimation uncertainty, respectively[16,17]. ECV estimates ranged from 441 to 460 ml. The average ECV of multiple DNH 155 reconstructions was 450 ml. The average ECV was similar when only based on each of the species of the reference sample separately (for the chimpanzee reference sample: 449 ml; for the gorilla reference sample: 452 ml; for the orangutan reference sample: 447 ml).

Simulating that the same regions as in DNH 155 were missing in each of the reference individuals and using the same methodology to estimate their ECV allowed comparison of the estimated and actual ECV and therefore an interpretation of how the choice of the reference sample influences the estimates[16,17]. This analysis (Supplementary Fig. 5) showed that for both multiple regression and multiple thin-plate spline reconstructions, the actual and predicted ECVs were highly correlated without a taxon-dependent bias towards overestimation or underestimation so that DNH 155's ECV could be estimated reliably. Furthermore, our results show that ECV estimates based on thin-plate spline reconstructions are consistent with regression-based estimates.

Principal component and cluster analyses. Nineteen measurements[59] were included in the analysis that could be measured in the best preserved *P. robustus* specimens, namely, DNH 7, DNH 155 and SK 48 (alveolar height, superior facial breadth, biorbital breadth, outer alveolar breadth, anterior interorbital breadth, orbital breadth, orbital height, minimum malar height, malar thickness, width of the temporal gutter, superior facial height, nasal height, rhinion-nasospinale, minimum frontal breadth, maxilloalveolar length, palate breadth, internal alveolar breadth at the M^3, P^3 interalveolar breadth, P^4 interalveolar breadth). Comparative data for chimpanzees were collected digitally from surface scans of a mixed subspecies sample (*Pan troglodytes schweinfurthii* curated at the Royal Museum of Central Africa and *Pan troglodytes troglodytes* curated at the Cleveland Museum of Natural History); data for fossil specimens other than DNH 155 and DNH 7 were taken from a published source[59]. The geometric mean of all 19 variables was calculated for each individual using Microsoft Excel's 'Geomean' function. Scale-adjusted shape indices[60] were then calculated for each of these 19 linear dimensions by dividing the original value by the geometric mean for that individual (Supplementary Materials).

A PCA was then performed on the shape indices in PAST v.3.12[61] and 19 principal components explaining 100% of the variation were extracted. The resultant principal component scores of the 19 principal components (Extended Data Fig. 6) were then used to perform a hierarchical cluster analysis using the paired group algorithm (unweighted pair group method with arithmetic mean (UPGMA)) and Euclidean distances. Note that PCA is not being used as a data reduction technique but rather to ensure that the variables in the UPGMA are statistically independent from one another and that the UPGMA accounts for the relative variation in each variable rather than simply the absolute variation[62]. Thus, the fact that DNH 7 is more similar to SK 48 than to DNH 155 on principal component 1 (explaining 34.5% of the total variance) does not outweigh the fact that DNH 7 and DNH 155 cluster together when considering all 19 principal components (explaining 100% of the variance).

Facial size. A prior assessment of sexual dimorphism in *P. robustus* relied heavily on a facial size index that represented an average of 12 linear dimensions[11]. Those measurements include: orbito-alveolar height; orbito-jugal height; foraminal height; alveolar height; bimaxillary breadth; interforaminal breadth; nasal aperture breadth; snout breadth; anterior maxilla-alveolar breadth; maxilla-alveolar breadth; palatal breadth; and post-canine maxilla-alveolar breadth. All of these measurements can be taken (in millimetres) on DNH 155 (orbito-alveolar height = 59; orbito-jugal height = 61; foraminal height = 36; alveolar height = 30; bimaxillary breadth = 93; interforaminal breadth = 51; nasal aperture breadth = 29; snout breadth = 56; anterior maxilla-alveolar breadth = 43; maxilla-alveolar breadth = 65; palatal breadth = 34; post-canine maxilla-alveolar breadth = 40). The average facial size value for DNH 155 is therefore 49.8 mm. This value is smaller than that recorded in any specimen from Swartkrans[11].

Metrical assessment of permanent maxillary dentition. Although all maxillary teeth are preserved in DNH 155, the tooth crowns are heavily worn and, in some cases, damaged such that standard dental metrics cannot be obtained for all teeth. In particular, interproximal wear is considerable on the post-canine teeth, so the mesiodistal (MD) dimension of the better-preserved antimere was estimated according to established methods[63]. MD and buccolingual (BL) dimensions in millimetres of the right (R) and left (L) maxillary teeth are as follows: RI^1 MD = 7.3, BL = 7.8; RI^2 MD = 5.6, BL = 6.8; RC MD = 7.2, BL = 9.8; RP^3 MD = 8.9 (9.8 estimated), BL = 13.2; RM^1 MD = 10.9 (12.1 estimated), BL = 14.7; RM^3 MD = 12.7 (14.4 estimated), BL = 15.3; LI^1 MD = 7.3, BL = 7.7; LI^2 MD = 5.6, BL = 6.8; LC MD = 7.2, BL = 9.6; LP^4 MD = 9.5 (10.3 estimated), BL = 13.5; LM^2 MD = 12.4 (13.8 estimated), BL = 14.7; LM^3 MD = 12.8, BL = 15.0.

A series of two-tailed Mann–Whitney *U*-tests were performed for the purposes of assessing size differences between the DMQ and Swartkrans *P. robustus* assemblages. The DMQ sample included DNH 155 (estimated values) as well as all previously published permanent maxillary *P. robustus* teeth from the DMQ[1,3,42] (Supplementary Table 4). Metrical data were drawn from these publications or, in the case of DNH 155, measured by the authors. The Swartkrans sample consisted of previously published permanent maxillary *P. robustus* teeth[9,64–69], including six isolated teeth measured by the authors (Supplementary Table 4). The Kromdraai B *P. robustus* specimens were not included in this analysis because the sample size was too small.

The Mann–Whitney *U*-tests were run in IBM SPSS Statistics v.25 (IBM Corporation) with the significance set at $P < 0.05$. The DMQ sample was significantly smaller than the Swartkrans sample with respect to both BL breadth and MD length for the P^3, P^4, M^2 and M^3 as well as the M^1 with respect to MD length (Extended Data Fig. 8 and Supplementary Table 5). The MD length of the I^1 and I^2 was also notably smaller at the DMQ than at Swartkrans, but not significantly so. These results update prior findings[42] that excluded DNH 7 and, naturally, could not have included DNH 155 or DNH 152[3].

Phylogenetic analysis. Character states for *P. robustus* from DMQ were added to an existing character matrix employed in a recent phylogenetic analysis of early hominins[70]. Character states for *Au. anamensis* derived from the recent description of the MRD-VP-1/1 cranium were also added[71], although modifications to the underlying character state definitions proposed therein were not adopted. In addition to the 15 fossil hominin operational taxonomic units, 5 extant hominoid species (*Homo sapiens, Pan troglodytes, Gorilla gorilla, Pongo pygmaeus, Hylobates*) were included as ingroup taxa in the phylogenetic analysis. *Colobus* and *Papio* were constrained as outgroup taxa.

This updated character matrix has been digitally archived and is available at http://morphobank.org/permalink/?P3477. A Bayesian inference analysis was conducted using MRBAYES v.3.2.6[72]. The standard model for Bayesian inference of phenotypic data (Markov *k*-state variable model with gamma-distributed rate variation) was used to account for the ascertainment bias of parsimony-informative morphological characters. The Markov chain Monte Carlo (MCMC) was run for 1 million generations using 4 chains (3 heated and 1 cold chain). Parameters were sampled every 1,000 generations. The first 30% of samples were discarded as burn-in. MCMC convergence was assessed using effective sample size values and the average s.d. of split frequencies, with convergence to stationary assumed for effective sample size values >200 and split frequencies below 0.01.

Following the standard Bayesian inference analysis, a Bayesian tip-dating approach was used to incorporate stratigraphic information into our estimation of relationships within the *Paranthropus* clade. Ingroup taxa for this analysis were limited to *P. aethiopicus*, *P. boisei*, *P. robustus* from Drimolen and *P. robustus* from other sites. An outgroup taxon was constructed for this analysis using the inferred ancestral states for the last common ancestor of the *Homo* + *Paranthropus* clade. As in the analysis described above, a Markov *k*-state variable prior was used to model morphological character evolution[73]. A fossilized birth–death (FBD) process was used as a prior on branch lengths[74–77]. By setting the sample strategy parameter 'rho' as equal to 1 in the FBD process, the analysis was run without sampled ancestors (that is, tip-dated). Following previous fossil tip-dating studies, the relaxed morphological clock assumed an independent gamma rate model[77–80]. Fossilization and speciation rate priors for the FBD process and the independent gamma rate model were defined using vague distributions (that is, uninformative priors). Priors on fossil occurrence dates were assigned uniform distributions to represent the maximally reported stratigraphic ranges (Supplementary Information). The MCMC was run for 3 million generations using 4 chains. Parameters were sampled every 5,000 generations. The first 30% of samples were discarded as burn-in. Convergence was assessed using the same procedures as those described above for the standard Bayesian inference analysis.

The complete 21 taxon character matrix was also analysed with maximum parsimony using PAUP* v.4[81]. A heuristic tree search was conducted by performing 1,000 replicates of Wagner trees using random addition sequences. This was followed by tree bisection and reconnection branch swapping. Ten trees were held per replicate. The character support of the most parsimonious reconstruction was calculated in PAUP* using character resampling techniques[82]. These bootstrap support values were calculated in an analysis of 10,000 replicates.

Reporting Summary. Further information on research design is available in the Nature Research Reporting Summary linked to this article.

Data availability

All data are available in the Methods, Supplementary Information and at MorphoBank (http://morphobank.org/permalink/?P3477). Specimen DNH 155 is curated by the Evolutionary Studies Institute of the University of the Witwatersrand. Requests for permission to examine DNH 155 should be directed to their hominin access committee and are subject to regulations of the South African Heritage Resources Agency.

Received: 8 July 2020; Accepted: 4 September 2020;
Published online: 09 November 2020

References

1. Keyser, A. W. The Drimolen skull: the most complete australopithecine cranium and mandible to date. *S. Afr. J. Sci.* **96**, 189–193 (2000).
2. Keyser, A. W., Menter, C. G., Moggi-Cecchi, J., Pickering, T. R. & Berger, L. R. Drimolen: a new hominid-bearing site in Gauteng, South Africa. *S. Afr. J. Sci.* **96**, 193–197 (2000).
3. Herries, A. I. R. et al. Contemporaneity of *Australopithecus*, *Paranthropus* and early *Homo erectus* in South Africa. *Science* **368**, eaaw7293 (2020).
4. Pickering, R. et al. U-Pb-dated fl wstones restrict South African hominin record to dry climate phases. *Nature* **565**, 226–229 (2019).
5. Broom, R. Another new type of fossil ape-man (*Paranthropus crassidens*). *Nature* **163**, 57 (1949).
6. Broom, R. & Robinson, J. T. *Swartkrans Ape-Man Paranthropus crassidens* (Transvaal Museum, 1952).
7. Grine, F. E. in *Ancestors: Th Hard Evidence* (ed. Delson, E.) 153–167 (Alan R. Liss, 1985).
8. Robinson, J. T. The genera and species of the Australopithecinae. *Am. J. Phys. Anthropol.* **12**, 181–200 (1954).
9. Robinson, J. T *The Dentition of the Australopithecinae* (Transvaal Museum, 1956).
10. Arnold, S. J. Morphology, performance and fitness. *Am. Zool.* **23**, 347–361 (1983).
11. Lockwood, C. A., Menter, C. G., Moggi-Cecchi, J. & Keyser, A. W. Extended male growth in a fossil hominin species. *Science* **318**, 1443–1446 (2007).
12. Rak, Y. *Th Australopithecine Face* (Academic Press, 1983).
13. Smith, A. L. et al. The feeding biomechanics and dietary ecology of *Paranthropus boisei*. *Anat. Rec. (Hoboken)* **298**, 145–167 (2015).
14. Ledogar, J. A. The biomechanics of bony facial "buttresses" in South African australopiths: an experimental study using fin te element analysis. *Anat. Rec. (Hoboken)* **300**, 171–195 (2017).
15. Kimbel, W. H., Rak, Y. & Johanson, D. C. *The Skull of Australopithecus afarensis* (Oxford Univ. Press, 2004).
16. Neubauer, S., Gunz, P., Weber, G. W. & Hublin, J.-J. Endocranial volume of *Australopithecus africanus:* new CT-based estimates and the effects of missing data and small sample size. *J. Hum. Evol.* **62**, 498–510 (2012).
17. Spoor, F. et al. Reconstructed *Homo habilis* type OH 7 suggests deep-rooted species diversity in early *Homo*. *Nature* **519**, 83–86 (2015).
18. Neubauer, S., Hublin, J.-J. & Gunz, P. The evolution of modern human brain shape. *Sci. Adv.* **4**, eaao5961 (2018).
19. Holloway, R. L., Broadfi ld, D. C. & Yuan, M. S. *The Human Fossil Record. Volume Three, Brain Endocasts, the Paleoneurological Evidence* (Wiley, 2004).
20. Johanson, D. C. & White, T. D. A systematic assessment of early African hominids. *Science* **203**, 321–330 (1979).
21. Walker, A., Leakey, R. E., Harris, J. M. & Brown, F. H. 2.5-Myr *Australopithecus boisei* from west of Lake Turkana, Kenya. *Nature* **322**, 517–522 (1986).
22. Kimbel, W. H., White, T. D. & Johanson, D. C. in *Evolutionary History of the "Robust" Australopithecines* (ed. Grine, F. E.) 259–258 (Aldine de Gruyter, 1988).
23. Wood, B. & Constantino, P. *Paranthropus boisei*: fi y years of fossil evidence and analysis. *Am. J. Phys. Anthropol.* **134**, 106–132 (2007).
24. Wood, B. A. & Schroer, K. in *Human Paleontology and Prehistory: Contributions in Honor of Yoel Rak* (eds Marom, A. & Hovers, E.) 95–107 (Springer, 2017).
25. Lehmann, J. & Boesch, C. Social influences on ranging patterns among chimpanzees (*Pan troglodytes verus*) in the Taï National Park, Côte d'Ivoire. *Behav. Ecol.* **14**, 642–649 (2003).
26. Pickering, R., Kramers, J. D., Hancox, P. J., de Ruiter, D. J. & Woodhead, J. D. Contemporary fl wstone development links early hominin bearing cave deposits in South Africa. *Earth Planet. Sci. Lett.* **306**, 23–32 (2011).
27. Herries, A. I. R. & Adams, J. W. Clarifying the context, dating and age range of the Gondolin hominins and *Paranthropus* in South Africa. *J. Hum. Evol.* **65**, 676–681 (2013).
28. Stammers, R., Caruana, M. & Herries, A. I. R. The fi st bone tools from Kromdraai and stone tools from Drimolen, and the place of bone tools in the South African Earlier Stone Age. *Quat. Int.* **495**, 87–101 (2018).
29. Bruxelles, L., Marie, R., Couzens, R., Thackeray, J. F. & Braga, J. in *Kromdraai: a birthplace of Paranthropus in the Cradle of Humankind* (eds Braga, J. & Thackeray, J. F.) 31–48 (Sun Press, 2016).
30. Leakey, M. G., Feibel, C. S., McDougall, I. & Walker, A. New four-million-year-old hominid species from Kanapoi and Allia Bay, Kenya. *Nature* **376**, 565–571 (1995).
31. Brunet, M. et al. *Australopithecus bahrelghazali*, une nouvelle espèce d'hominidé ancient de la région de Koro Toro (Tchad). *C. R. Acad. Sci.* **322**, 907–913 (1996).
32. Brunet, M. et al. A new hominid from the Upper Miocene of Chad, Central Africa. *Nature* **418**, 145–151 (2002).
33. Asfaw, B. et al. *Australopithecus garhi*: a new species of early hominid from Ethiopia. *Science* **284**, 629–635 (1999).
34. Senut, B. et al. First hominid from the Miocene (Lukeino Formation, Kenya). *C. R. Acad. Sci* **332**, 137–144 (2001).
35. Haile-Selassie, Y. H., Suwa, G. & White, T. D. Late Miocene teeth from Middle Awash, Ethiopia, and early hominid dental evolution. *Science* **303**, 1503–1505 (2004).
36. Berger, L. et al. *Australopithecus sediba*: a new species of *Homo*-like australopith from South Africa. *Science* **328**, 195–204 (2010).
37. Simpson, G. G. The species concept. *Evolution* **5**, 285–298 (1951).
38. de Queiroz, K. in *Endless Forms: Species and Speciation* (eds Howard, D. J. & Berlocher, S. H.) 57–75 (Oxford Univ. Press, 1998).
39. De Queiroz, K. Species concepts and species delimitation. *Syst. Biol.* **56**, 879–886 (2007).
40. Suwa, G., White, T. D. & Howell, F. C. Mandibular postcanine dentition from the Shungura Formation, Ethiopia: crown morphology, taxonomic allocations, and Plio-Pleistocene hominid evolution. *Am. J. Phys. Anthropol.* **101**, 247–282 (1996).

41. Kimbel, W. H. et al. Was *Australopithecus anamensis* ancestral to *A. afarensis*? A case of anagenesis in the hominin fossil record. *J. Hum. Evol.* **51**, 134–152 (2006).
42. Moggi-Cecchi, J., Menter, C., Boccone, S. & Keyser, A. Early hominin dental remains from the Plio-Pleistocene site of Drimolen, South Africa. *J. Hum. Evol.* **58**, 374–405 (2010).
43. Brain, C. K. *The Hunters or the Hunted? An Introduction to African Cave Taphonomy* (Univ. of Chicago Press, 1981).
44. Pickering, R. & Herries, A. I. R. in *Hominin Postcranial Remains from Sterkfontein, South Africa, 1936–1995*. (eds Zipfel, B., Richmond, B. & Ward, C. V.) 21–30 (Oxford Univ. Press, 2020).
45. Vrba, E. S. in *Ancestors: Th Hard Evidence* (ed. Delson, E.) 63–71 (Alan R. Liss, 1985).
46. Dupont, L. M., Donner, B., Vidal, L., Perez, E. M. & Wefer, G. Linking desert evolution and coastal upwelling: Pliocene climate change in Namibia. *Geology* **33**, 461–464 (2005).
47. Caley, T. et al. A two-million-year-long hydroclimatic context for hominin evolution in southeastern Africa. *Nature* **560**, 76–79 (2018).
48. Johannes-Boyau, R. et al. Elemental signatures of *Australopithecus africanus* teeth reveal seasonal dietary stress. *Nature* **572**, 122–115 (2019).
49. Pickering, R. et al. *Australopithecus sediba* at 1.977 Ma and implications for the origins of the genus *Homo*. *Science* **333**, 1421–1423 (2011).
50. Potts, R. Environmental hypotheses of hominin evolution. *Am. J. Phys. Anthropol.* **107**, 93–136 (1998).
51. Wood, B. & Strait, D. Patterns of resource use in early *Homo* and *Paranthropus*. *J. Hum. Evol.* **46**, 119–162 (2004).
52. Scott, R. S. et al. Dental microwear texture analysis shows within-species diet variability in fossil hominins. *Nature* **436**, 693–695 (2005).
53. Sponheimer, M. et al. Isotopic evidence for dietary variability in the early hominin *Paranthropus robustus*. *Science* **314**, 980–982 (2006).
54. Schroeder, L., Roseman, C. R., Cheverud, J. M. & Ackermann, R. R. Characterizing the evolutionary path(s) to early *Homo*. *PLoS ONE* **9**, e114307 (2014).
55. Mayr, E. *Systematics and the Origin of Species from the Viewpoint of a Zoologist* (Columbia Univ. Press, 1942).
56. Lordkipanidze, D. et al. A complete skull from Dmanisi, Georgia, and the evolutionary biology of early *Homo*. *Science* **342**, 326–331 (2013).
57. Neubauer, S., Gunz, P. & Hublin, J.-J. The pattern of endocranial ontogenetic shape changes in humans. *J. Anat.* **215**, 240–255 (2009).
58. Neubauer, S. & Gunz, P. in *Digital Endocasts: From Skulls to Brains* (eds Bruner, E. et al.) 173–190 (Tokyo Springer, 2018).
59. Wood, B. *Koobi Fora Research Project. Volume 4, Hominid Cranial Remains* (Clarendon Press, 1991).
60. Darroch, J. N. & Mossiman, J. E. Canonical and principal components of shape. *Biometrika* **72**, 241–252 (1985).
61. Hammer, Ø., Harper, D. A. T. & Ryan, P. D. PAST: paleontological statistics software package for education and data analysis. *Palaeontol. Electronica* **4**, 4 (2001).
62. Gordon, A. D., Nevell, L. & Wood, B. The *Homo floresiensis* cranium (LB1): size, scaling and early *Homo* affi ties. *Proc. Natl Acad. Sci. USA* **105**, 4650–4655 (2008).
63. Wood, B. A. & Engleman, C. A. Analysis of the dental morphology of Plio-Pleistocene hominids. V. Maxillary postcanine tooth morphology. *J. Anat.* **161**, 1–35 (1988).
64. Grine, F. E. New hominid fossils from the Swartkrans Formation (1979–1986 excavations): craniodental specimens. *Am. J. Phys. Anthropol.* **79**, 409–449 (1989).
65. Grine, F. E. & Daegling, D. New mandible of *Paranthropus robustus* from Member 1, Swartkrans Formation, South Africa. *J. Hum. Evol.* **24**, 319–333 (1993).
66. Grine, F. E. & Strait, D. S. New hominid fossils from Member 1 "Hanging Remnant", Swartkrans Formation, South Africa. *J. Hum. Evol.* **26**, 57–76 (1994).
67. Sutton, M. B. et al. Newly discovered fossil- and artefact-bearing deposits, uranium-series ages, and Plio-Pleistocene hominids at Swartkrans Cave, South Africa. *J. Hum. Evol.* **57**, 688–696 (2009).
68. Pickering, T. R. et al. New hominid fossils from Member 1 of the Swartkrans formation, South Africa. *J. Hum. Evol.* **62**, 618–638 (2012).
69. Pickering, T. R. et al. New early Pleistocene hominin teeth from the Swartkrans Formation, South Africa. *J. Hum. Evol.* **100**, 1–15 (2016).
70. Mongle, C. S., Strait, D. S. & Grine, F. E. Expanded character sampling underscores phylogenetic stability of *Ardipithecus ramidus* as a basal hominin. *J. Hum. Evol.* **131**, 28–39 (2019).
71. Haile-Selassie, Y., Melillo, S. M., Vazzana, A., Benazzi, S. & Ryan, T. M. A 3.8-million-year-old hominin cranium from Woranso-Mille, Ethiopia. *Nature* **573**, 214–219 (2019).
72. Huelsenbeck, J. P. & Ronquist, F. MRBAYES: Bayesian inference of phylogenetic trees. *Bioinformatics* **17**, 754–755 (2001).
73. Lewis, P. O. A likelihood approach to estimating phylogeny from discrete morphological character data. *Syst. Biol.* **50**, 913–925 (2001).
74. Pyron, R. A. Divergence time estimation using fossils as terminal taxa and the origins of Lissamphibia. *Syst. Biol.* **60**, 466–481 (2011).
75. Ronquist, F. et al. MrBayes 3.2: effici t Bayesian phylogenetic inference and model choice across a large model space. *Syst. Biol.* **61**, 539–542 (2012).
76. Gavryushkina, A., Welch, D., Stadler, T. & Drummond, A. J. Bayesian inference of sampled ancestor trees for epidemiology and fossil calibration. *PLoS Comput. Biol.* **10**, e1003919 (2014).
77. Heath, T. A., Huelsenbeck, J. P. & Stadler, T. The fossilized birth–death process for coherent calibration of divergence-time estimates. *Proc. Natl Acad. Sci. USA* **111**, E2957–E2966 (2014).
78. Wright, D. F. Bayesian estimation of fossil phylogenies and the evolution of early to middle Paleozoic crinoids (Echinodermata). *J. Paleontol.* **91**, 791–814 (2017).
79. Wright, D. F. & Toom, U. New crinoids from the Baltic region (Estonia): fossil tip-dating phylogenetics constrains the origin and Ordovician-Silurian diversifi ation of the Flexibilia (Echinodermata). *Palaeontology* **60**, 893–910 (2017).
80. Zhang, C., Stadler, T., Klopfstein, S., Heath, T. A. & Ronquist, F. Total-evidence dating under the fossilized birth–death process. *Syst. Biol.* **65**, 228–249 (2016).
81. Swofford, D. L. *PAUP*: Phylogenetic Analysis Using Parsimony (*and Other Methods). Version 4.0a* (Sinauer Associates, 2002).
82. Felsenstein, J. Confide ce limits on phylogenies: an approach using the bootstrap. *Evolution* **39**, 783–791 (1985).

Acknowledgements

We thank Y. Rak and B. Kimbel, who are completing a detailed description of the DNH 7 skull, for sharing observations and insights on this specimen, a number of which correspond to ours; however, endorsement of our conclusions is not implied and all observations and interpretations are, of course, our own. The research underpinning this publication was undertaken while J.M.M. and A.B.L. were completing a PhD at La Trobe University. We thank the student excavators from the Washington University Drimolen Cave Field School and the Australian Palaeoanthropological Fieldschool at Drimolen. We dedicate the discovery of DNH 155 to I. Good, whose daughter S. Good uncovered the specimen on Father's Day in 2018. We thank R. Nsibande for invaluable logistical assistance and we remember S. Mokobane for many years of similar support as well as mentorship and friendship but who sadly died mere months before the discovery of DNH 155. We thank J. Massey for providing access to digital data, K. McNulty and A. Gordon for providing statistical advice and support, A. Larson for advice regarding species concepts and to J.-J. Hublin and P. Gunz for access to data and support. We thank D. Wright for methodological assistance with the tip-dated analysis. We thank J. Adams and M. Meredith-Williams for the supervision provided to J.M.M. and A.B.L. throughout their PhD programmes (in addition to that also provided by A.I.R.H. and D.S.S.). We also thank P. Strait for timely advice regarding probability theory. We thank the landowners (K. and N. Nkosi) for their continuing support to excavate at Drimolen, including through South African Heritage Resource Agency permit nos. 2597 and 2883 to S.E.B. and A.I.R.H. This research was funded and supported by Higher Degree Research fee waivers and living scholarships from La Trobe University to J.M.M. and A.B.L. and an Australian Research Council Discovery Grant no. DP170100056 to A.I.R.H. and D.S.S. Biomechanical analysis was supported by a grant to D.S.S. from the Biological Anthropology Directorate of the National Science Foundation (no. NSF-BCS-0725126). S.N. was supported by the Max Planck Society.

Author contributions

A.B.L., S.E.B., A.I.R.H., J.M.M., G.B. and D.S.S. participated in the recovery of DNH 155 and J.M.M. and A.B.L. reconstructed the specimen. A.B.L., J.M.M., S.N., C.S.M., G.T.S. and D.S.S. analysed and described the morphology. A.L.S., J.A.L. and D.S.S. conducted the biomechanical analyses of early hominins. A.I.R.H. and G.B. assessed the depositional context and age of the specimen. All authors wrote the paper.

Competing interests

The authors declare no competing interests.

Additional information

Extended data is available for this paper at https://doi.org/10.1038/s41559-020-01319-6.

Supplementary information is available for this paper at https://doi.org/10.1038/s41559-020-01319-6.

Correspondence and requests for materials should be addressed to D.S.S.

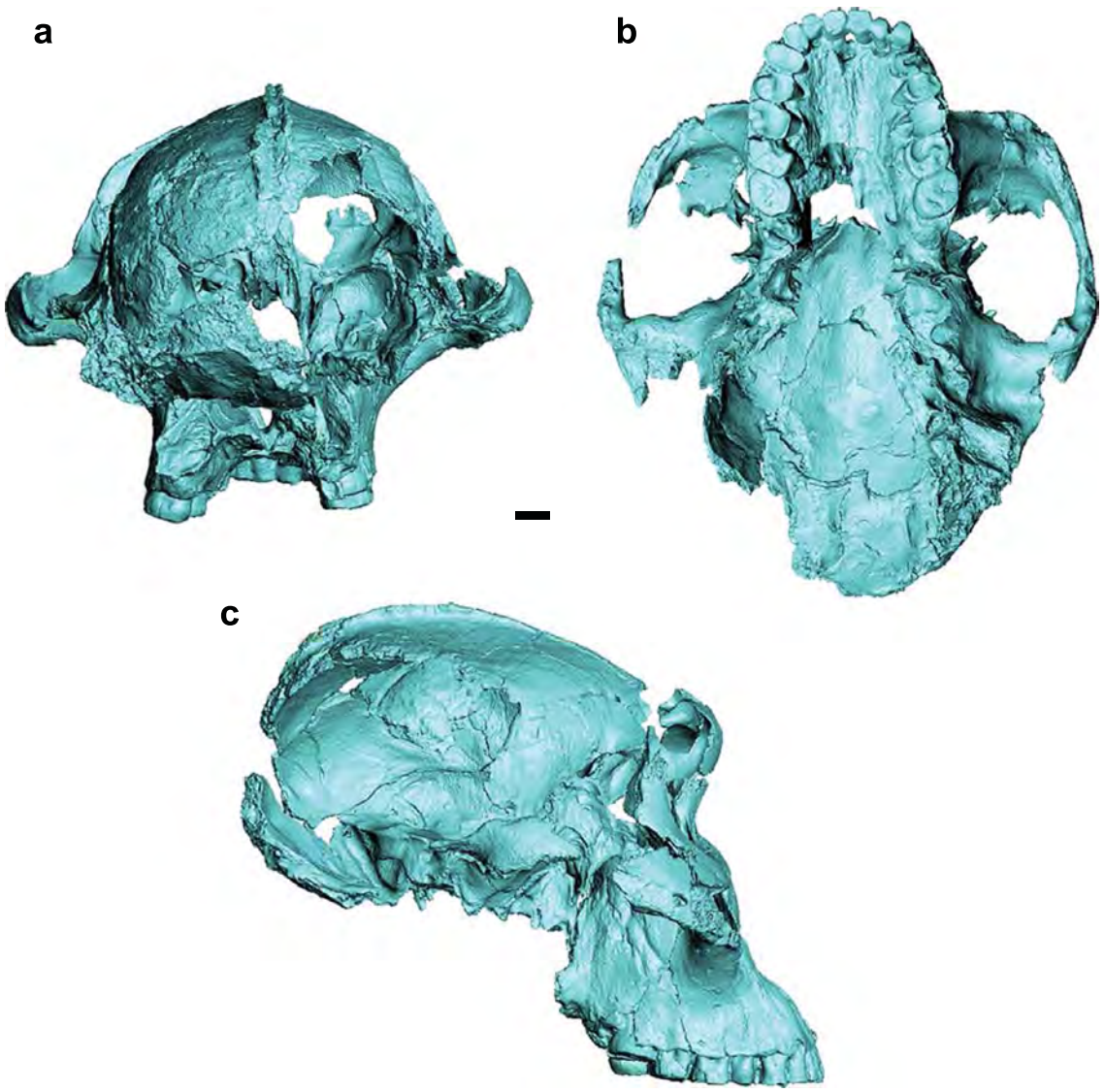

Extended Data Fig. 1 | Surface scans of DNH 155. Specimen positioned in **a**, posterior, **b**, basal, and **c**, right lateral views. Scale bar = 10mm.

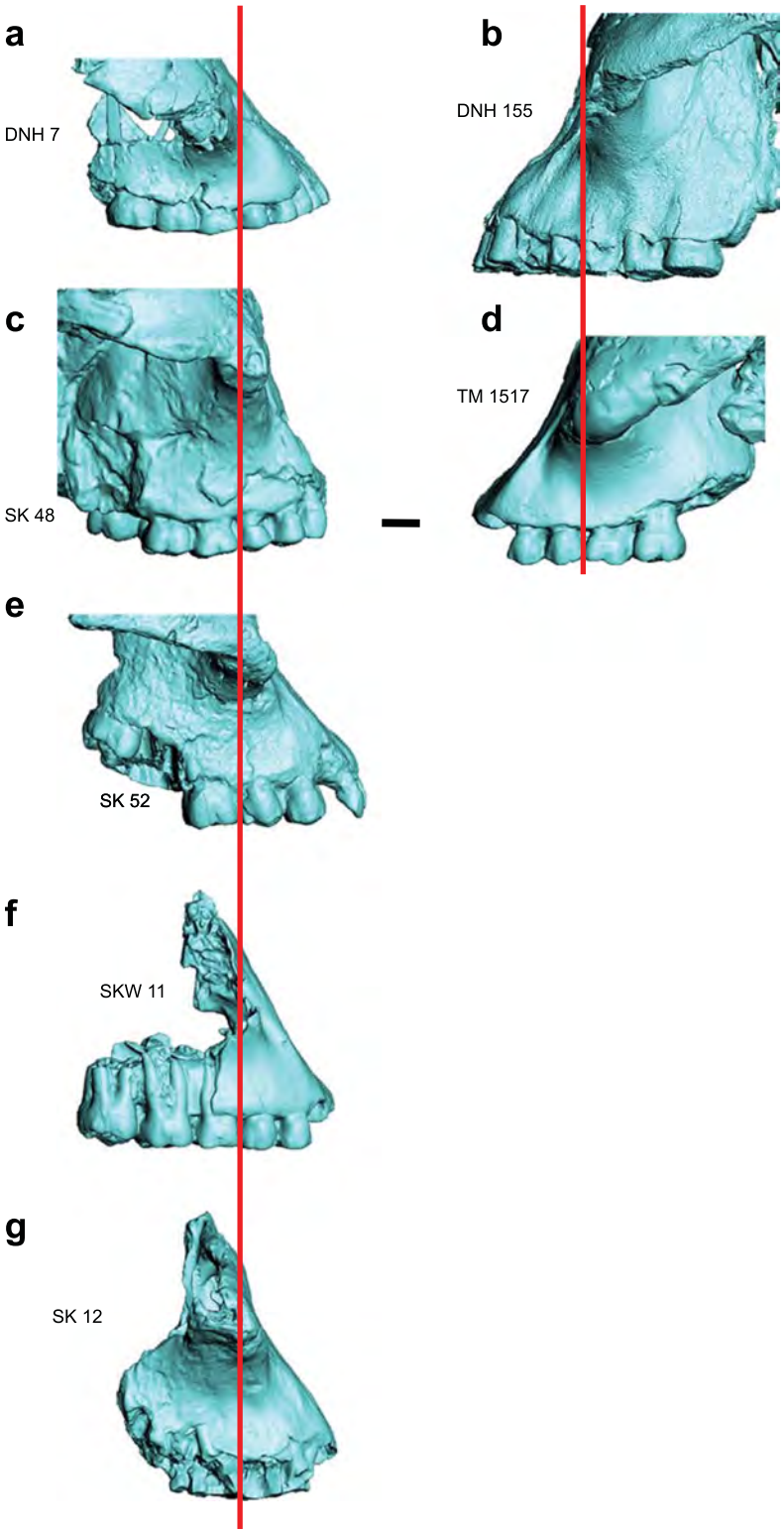

Extended Data Fig. 2 | Position of the zygomatic root. Right lateral views of *P. robustus* specimens **a**, DNH 7, **c**, SK 48, **e**, SK 52, **f**, SKW11, and **g**, SK 12. Left lateral views of **b**, DNH 155, and **d**, TM 1517. Vertical red lines pass through P^4/M^1 on each specimen. The anterior aspect of the root is positioned at this line in **a** and **b** but anterior to the line in **c**–**g**. Scale bar = 10mm.

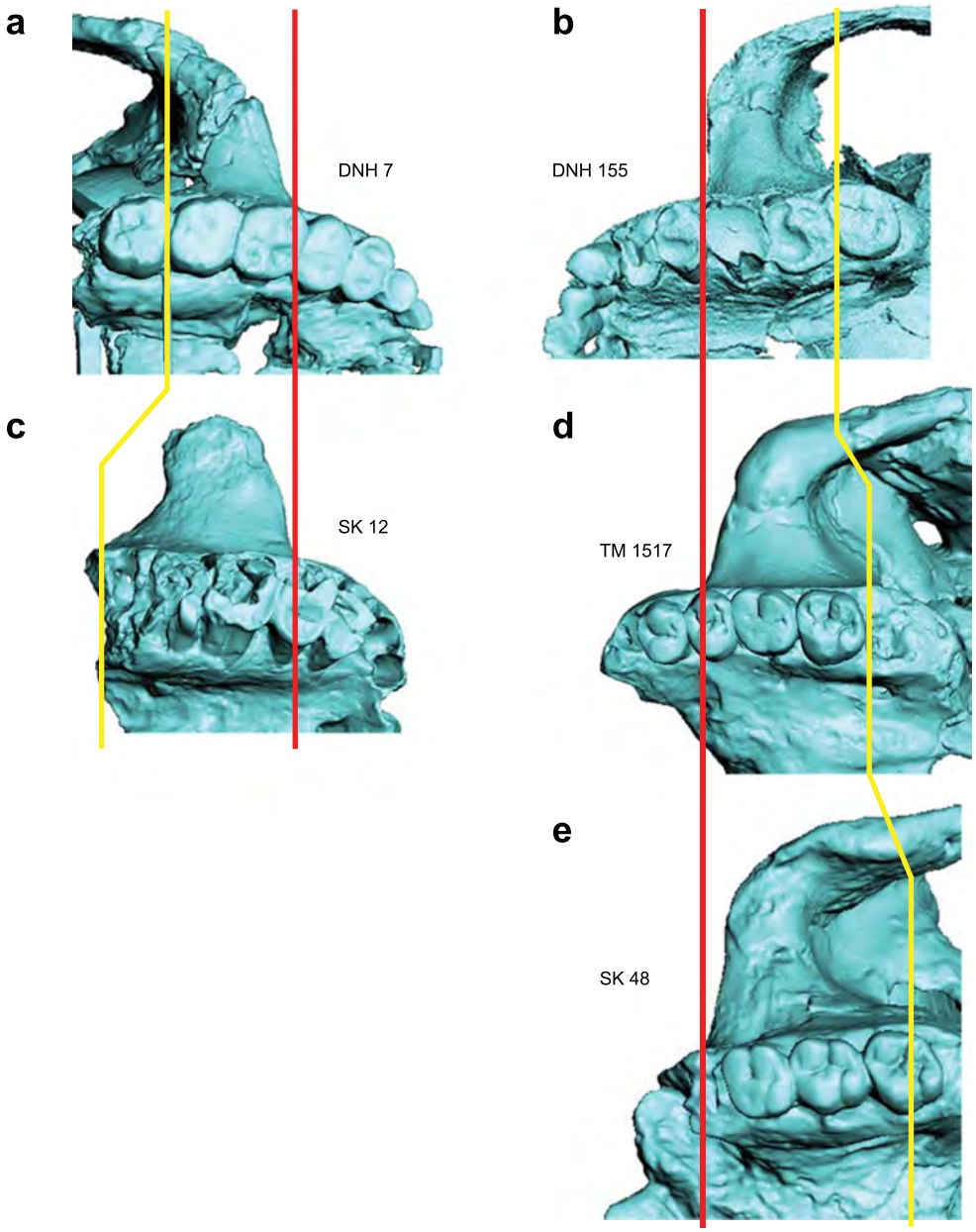

Extended Data Fig. 3 | Thickness of the zygomatic root. *Paranthropus robustus* specimens shown slightly offset from palatal view in order to visualize the lateral wall of the maxilla. **a**, DNH 7. **b**, DNH 155. **c**, SK 12. **d**, TM 1517. **e**, SK 48. All specimens are scaled to the same P^4 – M^2 length. Red and yellow lines represent the anterior- and posterior-most aspects of the zygomatic root on the maxilla. The root is proportionally thinnest in DNH 7 and DNH 155.

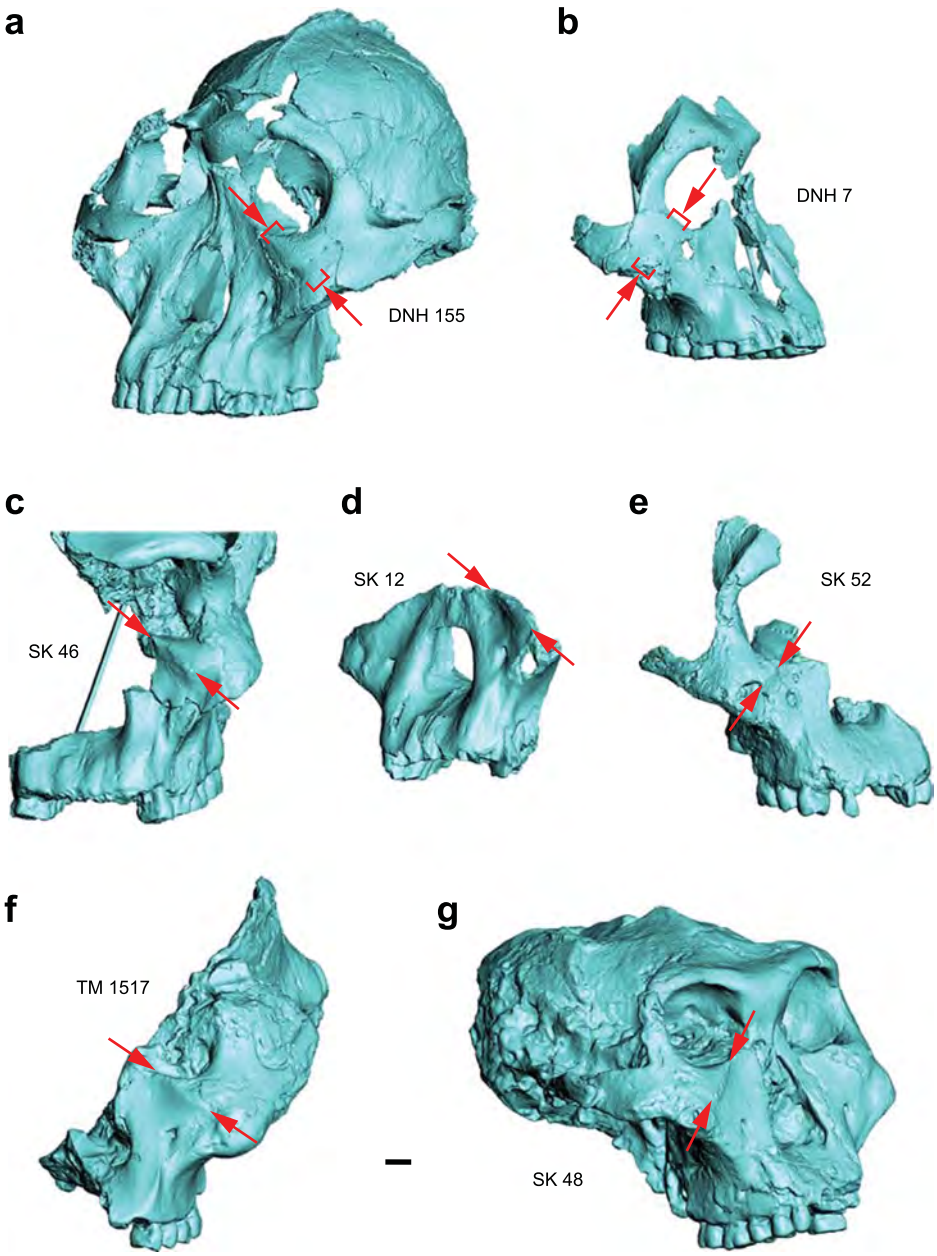

Extended Data Fig. 4 | Zygomaticomaxillary step. Oblique views of *P. robustus* specimens **a**, DNH 155, **b**, DNH 7, **c**, SK 46, **d**, SK 12, **e**, SK 52, **f**, TM 1517, and **g**, SK 48. Arrows indicate change of contour between the surfaces of the zygomatic bone and maxillary trigon. Shading indicates that the change in contour is abrupt and coincident with the zygomaticomaxillary suture in **c**–**g**, In **a** and **b** the change in contour is gentle (brackets) and positioned above the suture such that the suture lies within the trigon as opposed to being its superolateral margin. Scale bar = 10mm.

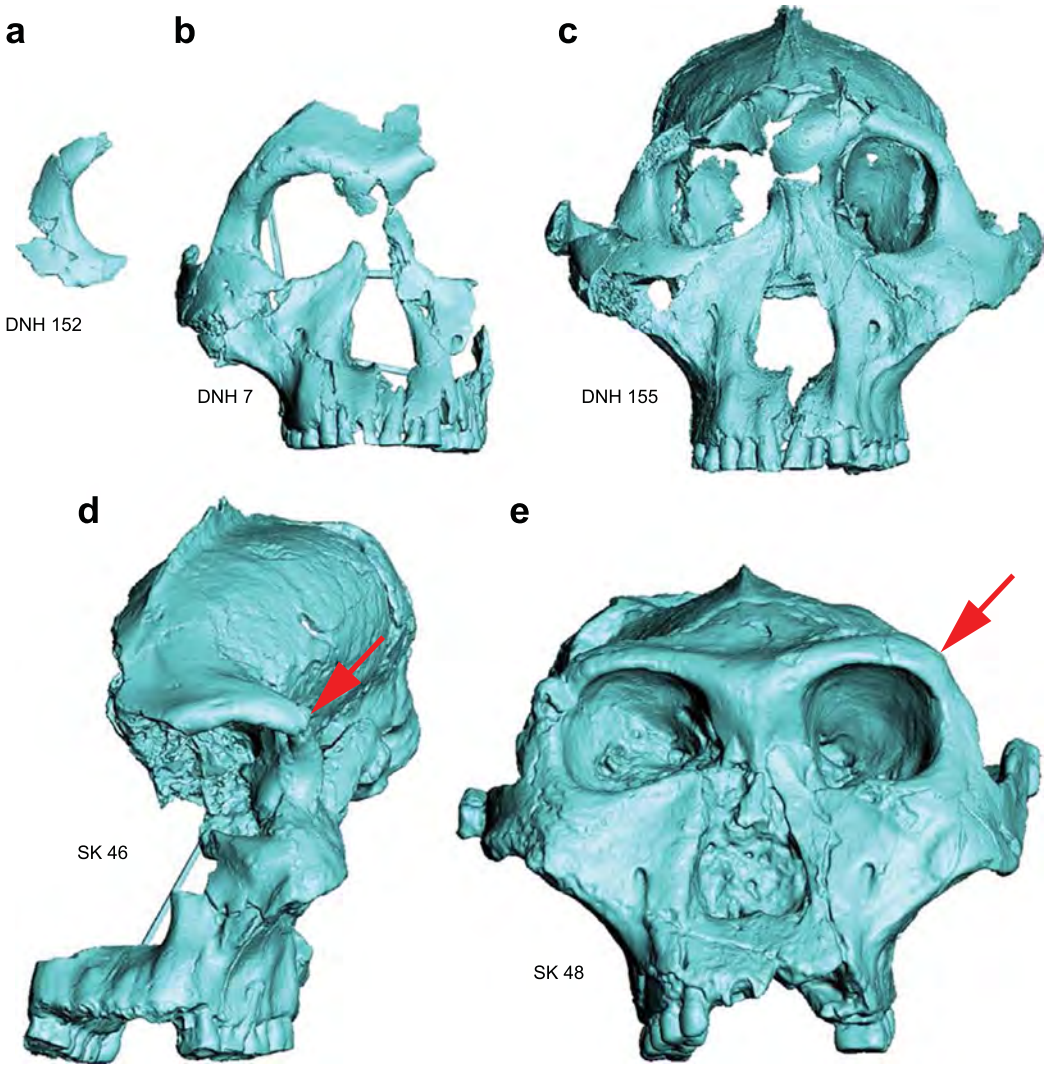

Extended Data Fig. 5 | Supraorbital corner. Frontal views of *P. robustus* specimens **a**, DNH 152, **b**, DNH 7, **c**, DNH 155, **d**, SK 46, and **e**, SK 48. Arrows indicate a squared supraorbital corner associated with a roughly horizontal supraorbital torus in **d** and **e**. In **a** and **b** the homologous region of the orbital margin is rounded, and in **c** the corner is not squared and the supraorbital torus is inclined. Note that specimen SK 46 is badly distorted, but the torus and corner are locally undistorted. Images not to the same scale.

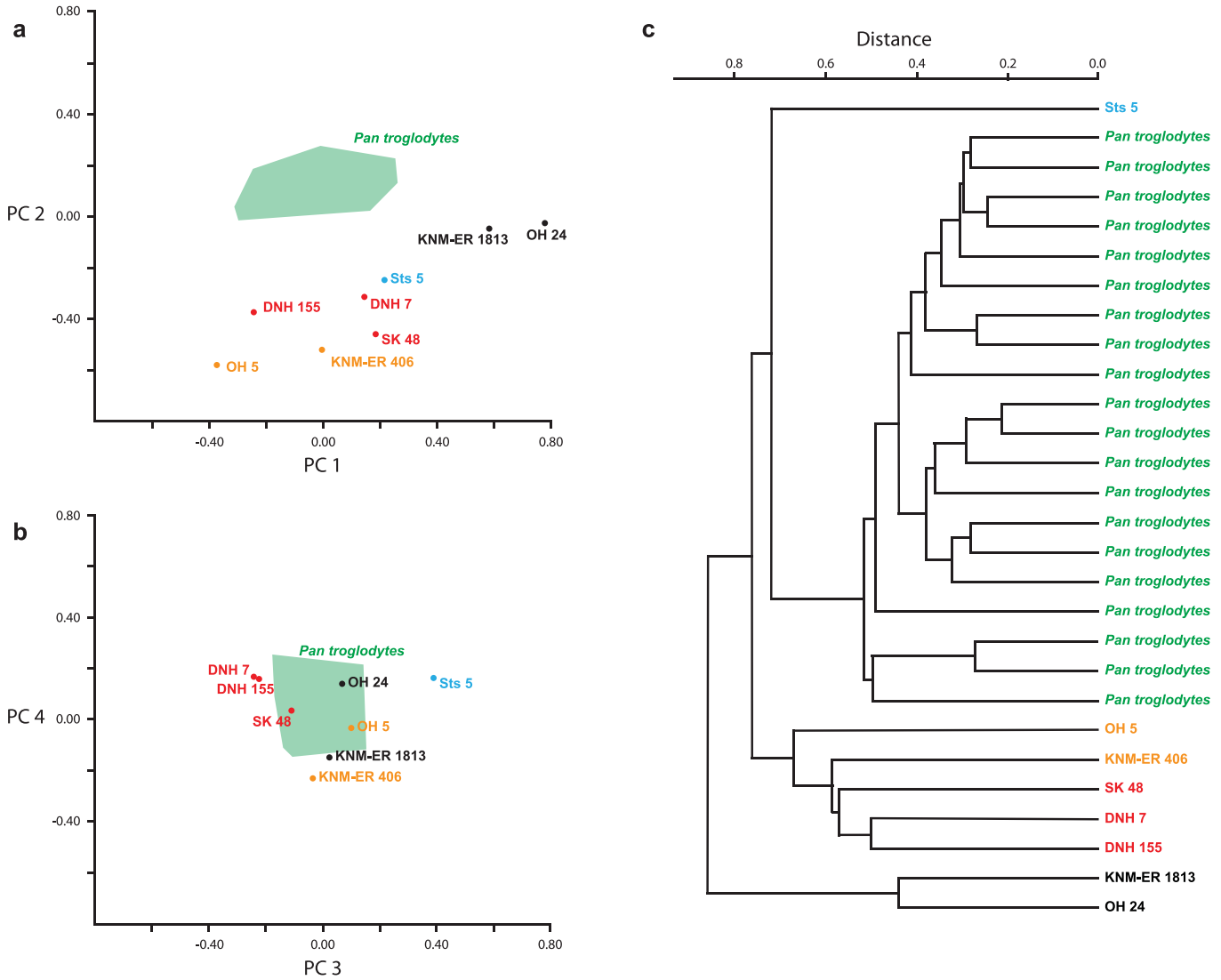

Extended Data Fig. 6 | Principal component and cluster analysis. Principal component analysis of 19 scale-adjusted craniofacial dimensions (Supplementary Data) were performed on chimpanzees (green) and fossil hominins (*P. robustus* = red, *P. boisei* = orange, *Au. africanus* = blue, early *Homo* = black) in order to convert the morphometric data into statistically independent variables to be used as input for cluster analysis. **a**, Plot of PC1 vs. PC2. **b**, PC3 vs. PC 4. PC 1 accounts for 34.5% of the total variance, PC2 for 28.5%, PC3 for 8.5%, and PC4 for 7.6%. PC1 and PC4 reflect interactions between facial height and minimum frontal breadth, albeit in inverse ways (PC1 loadings: Scale-adjusted Superior Facial Height = -0.51, Scale-Adjusted Nasal Height = -0.43, Scale-Adjusted Minimum Frontal Breadth = 0.44; PC4 loadings: Scale-adjusted Superior Facial Height = 0.41, Scale-Adjusted Minimum Frontal Breadth = 0.49). PC2 reflects palate shape (PC2 loadings: Scale-adjusted Outer Alveolar Breadth = -0.41, Scale-adjusted Interalveolar Distance at P^3 = 0.43). PC3 reflects alveolar shape (PC3 loadings: Scale-adjusted Alveolar Height = 0.39, Scale-adjusted Maxilloalveolar length = 0.41). **c**, Dendrogram of UPGMA of the 19 sets of component scores (accounting for 100% of the total variance) showing that DNH 155 clusters with DNH 7 within *P. robustus* and *Paranthropus* clusters.

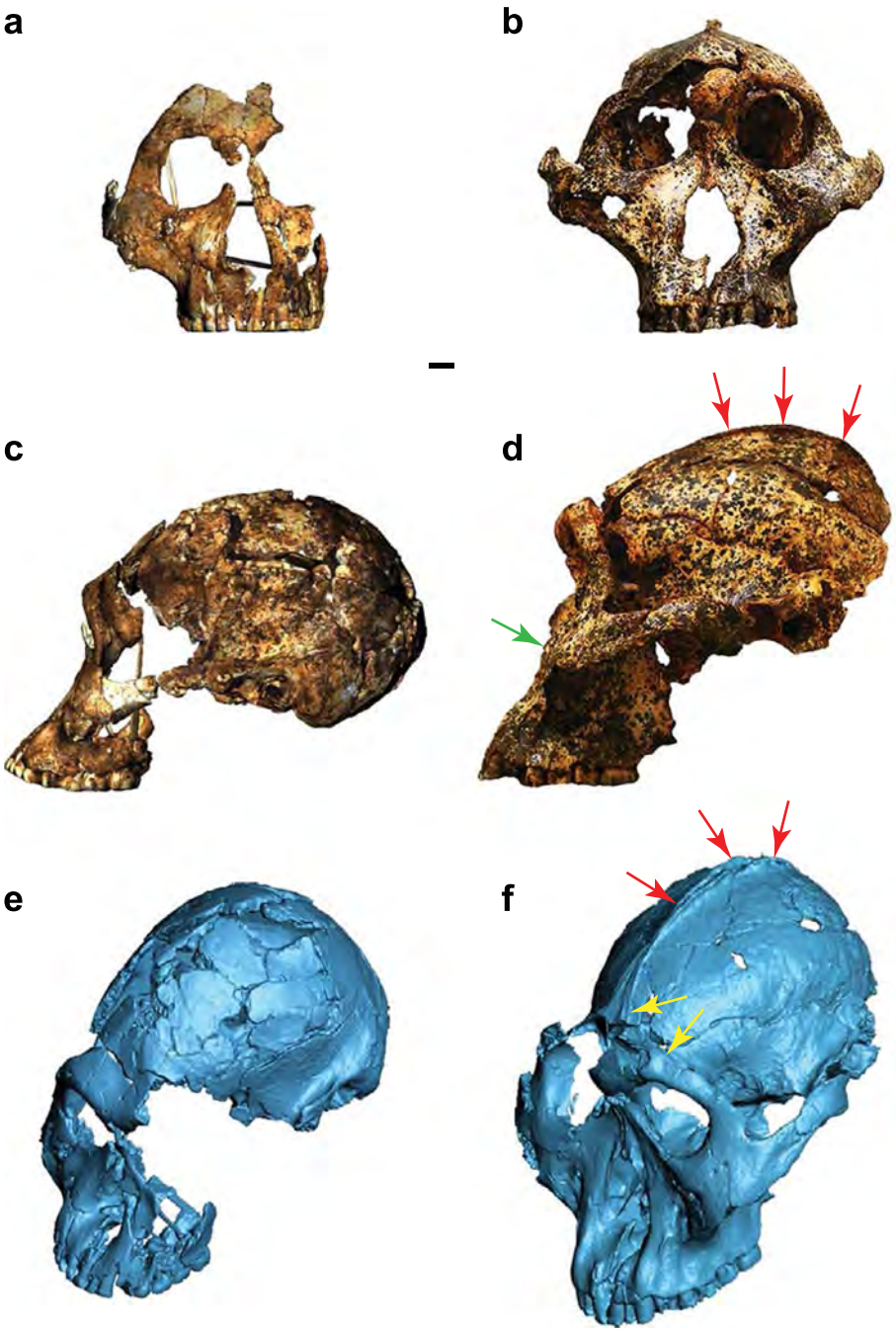

Extended Data Fig. 7 | Sexual dimorphism in *P. robustus* from DMQ. Frontal (top row), lateral (middle row) and superior-oblique (bottom row) views of **a**, **c**, **e**, DNH 7 and **b**, **d**, **f**, DNH 155. Note that the face of DNH 7 is detached from the specimen's neurocranium and neurocranial distortion makes it difficult to join the two pieces. The placement of the face on the neurocranium in lateral and oblique views is heuristic and no morphological assessments reported here are dependent on these cranial parts being properly aligned. Moreover, the lateral view of DNH 7 is a reflected image of the specimen's right side. DNH 155 is absolutely larger than DNH 7, it exhibits a sagittal crest (red arrows) and strong anteromedial incursion of the superior temporal lines (yellow arrows), and a zygomatic body that projects anterior to the nasal aperture (green arrow). DNH 7 is smaller, it lacks a sagittal crest, has only moderate anteromedial incursion of the superior temporal lines, and its zygomatic body does not project anterior to the nasal aperture. Scale bar = 10mm. Oblique views not to scale.

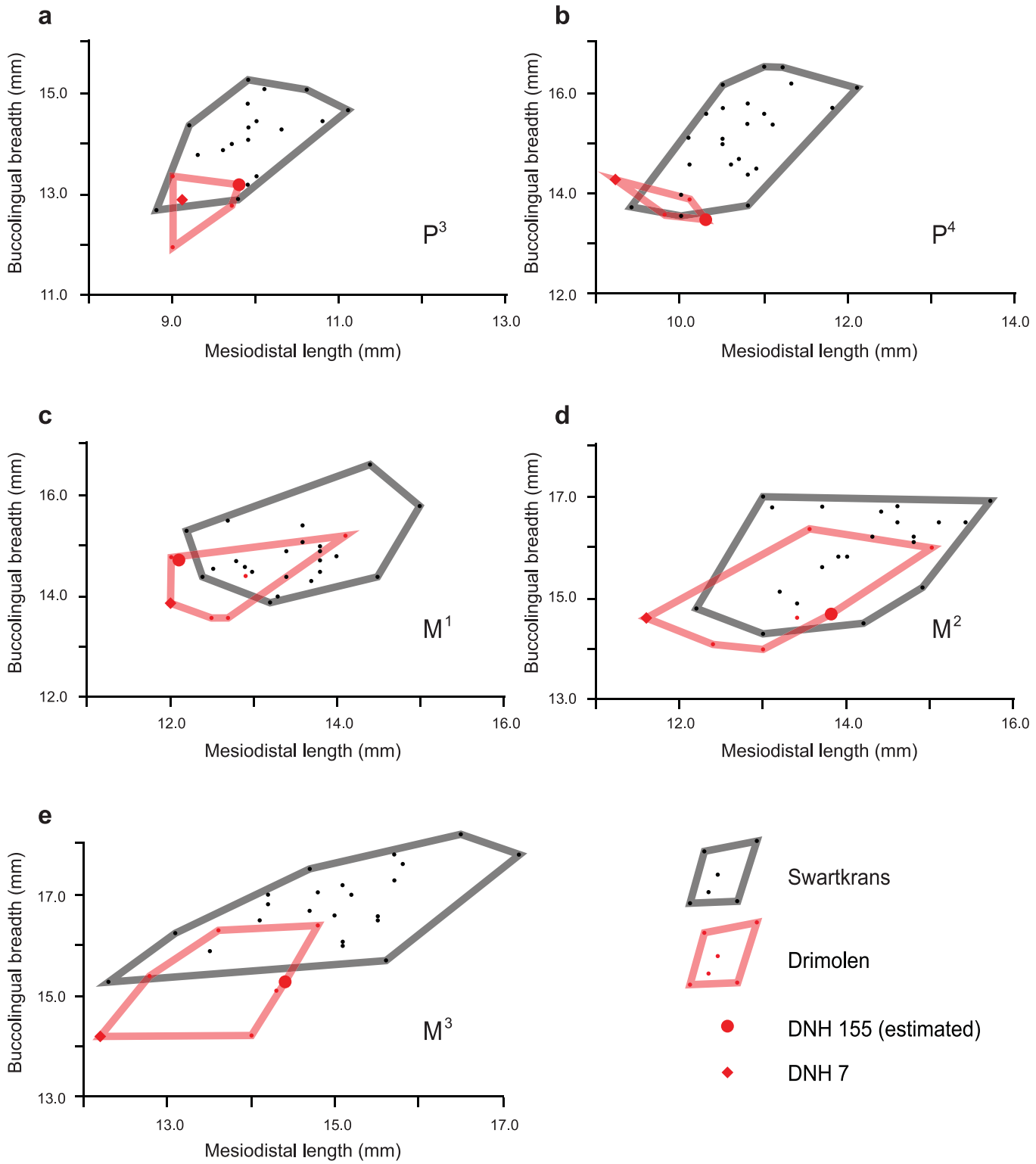

Extended Data Fig. 8 | Postcanine tooth size. Buccolingual breadth vs. mesiodistal length of *P. robustus* postcanine teeth at Drimolen and Swartkrans. **a**, P^3. **b**, P^4. **c**, M^1. **d**, M^2. **e**, M^3. Values for specimen DNH 155 are corrected for interproximal wear.